

Optimal collision energy for realizing macroscopic high baryon-density matter

Hidetoshi Taya,^{1,2,*} Asanosuke Jinno,^{3,†} Masakiyo Kitazawa,^{4,5,‡} and Yasushi Nara^{6,§}¹*Department of Physics, Keio University, 4-1-1 Hiyoshi, Kanagawa 223-8521, Japan*²*RIKEN iTHEMS, RIKEN, Wako 351-0198, Japan*³*Department of Physics, Faculty of Science, Kyoto University, Kyoto 606-8502, Japan*⁴*Yukawa Institute for Theoretical Physics, Kyoto University, Kyoto, 606-8317, Japan*⁵*J-PARC Branch, KEK Theory Center, Institute of Particle and Nuclear Studies, KEK, 319-1106, Japan*⁶*Akita International University, Yuwa, Akita-city 010-1292, Japan*

(Dated: September 13, 2024)

We investigate the volume and lifetime of the high baryon-density matter created in heavy-ion collisions and estimate the optimal collision energy to realize the high baryon-density region over a large spacetime volume. We simulate central collisions of gold ions for the center-of-mass energy per nucleon pair $\sqrt{s_{NN}} = 2.4 - 19.6$ GeV with a microscopic transport model JAM. We discover that the optimal collision energy is around $\sqrt{s_{NN}} = 3 - 4$ GeV, where a baryon density exceeding three times the normal nuclear density is realized with a substantially large spacetime volume. Higher and lower energies are disfavored due to short lifetime and low density, respectively. We also point out that event-by-event fluctuations of the spacetime density profile are large, indicating the importance of the event selection in the experimental analysis.

Introduction.— Exploring the properties of matter at extremely high baryon densities that exceed several times the normal nuclear density $\rho_0 \approx 0.17 \text{ fm}^{-3}$ is one of the most exciting frontiers in current physics. Such a high density environment is realized in, for example, the core of neutron stars. Recent remarkable progress in the observation of neutron stars through gravitational waves from binary neutron-star mergers [1] and pulsar X-rays [2] provides valuable information for constraining the equation of state of the dense matter [3]. The form of matter in such extreme conditions is determined by quantum chromodynamics (QCD) — the theory of strong interaction — and is expected to have rich phase structure [4]. Unveiling their properties is one of the ultimate goals of nuclear physics. Experimental inputs are crucial to achieve this, since the first-principle lattice-QCD calculation is difficult due to the notorious sign problem [5] and the low-energy effective models, such as the chiral effective theory, become invalid when the baryon density exceeds about $2\rho_0$ [6–8].

Relativistic heavy-ion collisions are the only terrestrial experiments to create such high baryon-density matter and to study their properties in laboratories [9]. In these experiments, dense and hot matter is created by colliding heavy nuclei accelerated up to almost the speed of light with a large accelerator. The experiments have been carried out at various facilities such as the LHC [10], RHIC [11], and SIS18 [12], for a wide range of collision energies with the center-of-mass energy per nucleon pair $\sqrt{s_{NN}}$ up to 5 TeV. In the past decades, the high energy region $\sqrt{s_{NN}} \gtrsim 100$ GeV has been extensively investigated at the LHC and RHIC. They are suitable for creating extremely hot but low baryon-density matter, and have succeeded in reproducing the primordial form of matter of the Universe just after the Big Bang — the quark-gluon plasma [13]. Recently, the lower energy

range $\sqrt{s_{NN}} \approx 3 - 20$ GeV, which we call *intermediate collision energies*, is attracting renewed attention. The intermediate energies are expected to be suitable for exploring high baryon-density and low-temperature matter, which is crucial to understand the interiors of neutron stars and supernovae. This energy range is actively investigated in the Beam-Energy Scan (BES) program at RHIC [14] and NA61/SHINE at SPS [15], and will be further studied worldwide [16] in NICA [17], FAIR [18], HIAF [19], and J-PARC-HI [20], which will drastically improve the statistics.

Several experimental results support the formation of high baryon-density matter at the intermediate energy region. First, the rapidity distribution of net-proton number in collisions of gold (Au) nuclei at $\sqrt{s_{NN}} = 5 - 200$ GeV [21] implies strong stopping of baryon charges at mid-rapidity for the AGS energy $\sqrt{s_{NN}} \approx 5$ GeV and hence realization of high baryon density. Second, a more quantitative estimate is feasible with the thermal-statistical fit to the hadron yields. It has been estimated in Ref. [22] that the baryon density at the chemical freeze-out is maximized at $\sqrt{s_{NN}} \approx 8$ GeV. However, it is *not* the maximum baryon density for a whole heavy-ion reaction, since the chemical freezeout occurs at a late stage, where the baryon density is diluted by the expansion.

To investigate the maximum baryon density, one must resort to dynamical models of heavy-ion collisions, such as microscopic transport models [23–26], hydrodynamic models [27–30], and hybrid models [31–34]. Previous microscopic transport-model calculations predicted that the maximum baryon density *at the center* of the collision system can exceed $8\rho_0$ for $\sqrt{s_{NN}} \gtrsim 5$ GeV [35–38]. It has also been discussed that even higher densities over $10\rho_0$ can be reached in some collision events due to large event-by-event fluctuations [37]. However, these studies focus on the density at the center, and *it is unclear how*

much the dense region extends in space and time. The large spatial and temporal sizes, besides the maximum baryon density, are crucial for the dense matter to leave observable signals in the final state. Despite its importance, to the best of our knowledge, quantitative studies on the volume and lifetime of the dense region and their dependence on $\sqrt{s_{NN}}$ have not been performed.

The purpose of this letter is to examine the spacetime volume of the high baryon-density region in intermediate-energy heavy-ion collisions and to estimate the optimal collision energy that maximizes the spacetime volume.

Measures.— To quantify the volume and lifetime of the high-baryon-density region in heavy-ion collisions, we propose the following three measures. These measures are constructed from the baryon density in the local rest frame (Eckart frame) [39],

$$\rho(x) := \sqrt{J^\mu(x)J_\mu(x)}, \quad (1)$$

where $J^\mu(x)$ is the baryon current at each spacetime point x in the center-of-mass frame of a collision system.

The first measure is the spatial volume that exceeds a threshold density value ρ_{th} ,

$$V_3(\rho_{th}; t) := \int_{\rho(x) > \rho_{th}} d^3\mathbf{x} \gamma[J(x)]. \quad (2)$$

The Lorentz factor $\gamma[J(x)] := 1/\sqrt{1 - (\mathbf{J}(x)/J^0(x))^2}$ is inserted to define the volume in the local rest frame. Second, we introduce a Lorentz invariant four-volume $V_4(\rho_{th})$ as [40]

$$V_4(\rho_{th}) := \int_{\rho(x) > \rho_{th}} dt d^3\mathbf{x}. \quad (3)$$

Finally, we define a measure of the typical lifetime of the dense region as

$$\tau(\rho_{th}) := \frac{V_4(\rho_{th})}{\max[V_3(\rho_{th}; t)]}, \quad (4)$$

where $\max[V_3(\rho_{th}; t)]$ is the maximum of $V_3(\rho_{th}; t)$ over time. We compute Eqs. (2)–(4) on an event-by-event basis, i.e., they are constructed from $J^\mu(x)$ for each event.

The advantages of the measures are their simplicity and the clarity of the physical meanings. They can be calculated straightforwardly in a given dynamical model without any further assumptions, once $J^\mu(x)$ is given. However, these measures are not concerned with the local equilibration, and hence the local temperature and/or the chemical potential. Whereas local equilibration has been studied within some microscopic transport models [41–46], it must introduce criteria for equilibration in a finite and dynamical system, leaving ambiguities in the analysis/interpretation.

Nevertheless, we emphasize that these measures can constrain the spacetime profile of the equilibrated region,

since $V_3(\rho_{th}, t)$ and $V_4(\rho_{th})$ obviously give the upper limits for the spacetime volumes of the equilibrated region. Furthermore, the formation of the dense region is of interest even without equilibration because such a high density can induce intriguing phenomena, such as the chiral vortical effect [47] and the nucleation of deconfined regions.

Simulation method.— We investigate the $\sqrt{s_{NN}}$ dependence of the measures (2)–(4) in central Au+Au collisions. We employ a microscopic transport model JAM [48, 49] and generate 1000 collision events with the impact parameter less than 3 fm, which roughly corresponds to the top 5% centrality cut. The simulations are performed with version 2.5743 in the default setting, unless otherwise stated. This version incorporates the recently implemented covariant cascade algorithm [50] and the Lorentz-vector version of the relativistic molecular dynamics (RQMDv) with the mean field of the soft momentum-dependent potential [51, 52]. As shown in Refs. [51, 52], RQMDv can successfully reproduce various experimental data, such as the collision energy dependencies of the directed flows of protons and Λ over a wide range of collision energies.

To define the baryon current $J^\mu(x)$ as a continuous quantity, we smear the baryon density of particles at position X_b and momentum P_b^μ as $J^\mu(x) := \sum_{b \in \text{baryons}} V_b^\mu B_b g(x - X_b; P_b)$, where B_b and $V_b^\mu = P_b^\mu/P_b^0$ are the baryon number and velocity of the b -th baryon [53], respectively, and $g(x; P) := \gamma[P]/(\sqrt{2\pi}r)^3 \exp[-(|\mathbf{x}|^2 + (\gamma[P]\mathbf{V}_b \cdot \mathbf{x})^2)/(2r^2)]$ is a relativistic Gaussian smearing function [54, 55]. We use the smearing width $r = 1$ fm for all baryons, which is almost the same size as the charge radius of protons [56]. The smearing can be interpreted as the intrinsic distribution of baryon density inside baryons or a technical coarse-graining for numerics. The maximum value of the smearing function $g(0; 0) \approx 0.37\rho_0$ is much smaller than ρ_0 , indicating that a considerable number of baryons must overlap to realize $\rho(x) \gg \rho_0$.

Simulation results.— Figure 1 shows the time dependence of $V_3(\rho_{th}; t)$ for various collision energies. The thick-solid, thin-dashed, and dotted lines show, respectively, the results from the full simulation with the mean field (MF), the cascade mode (Cascade), where the mean field is turned off, and the free streaming (FS) simulations, where all the interactions are switched off.

One observes that $V_3(\rho_{th}; t)$ for $\rho_{th}/\rho_0 = 3$ has the maximum value $(\max[V_3(\rho_{th}; t)])^{1/3} \approx 6$ fm for all collision energies. We regard this length scale as “macroscopically” large, since it is much larger than the typical microscopic length scale of the system ≈ 1 fm, determined by the interaction range and the sizes of hadrons. Additionally, the achieved length scale is comparable to the radius of the colliding gold ions $R_{Au} \approx 6.4$ fm and thus is “maximally” large in the sense that the overlap of two nuclei cannot result in a volume larger than $\approx R_{Au}^3$. Re-

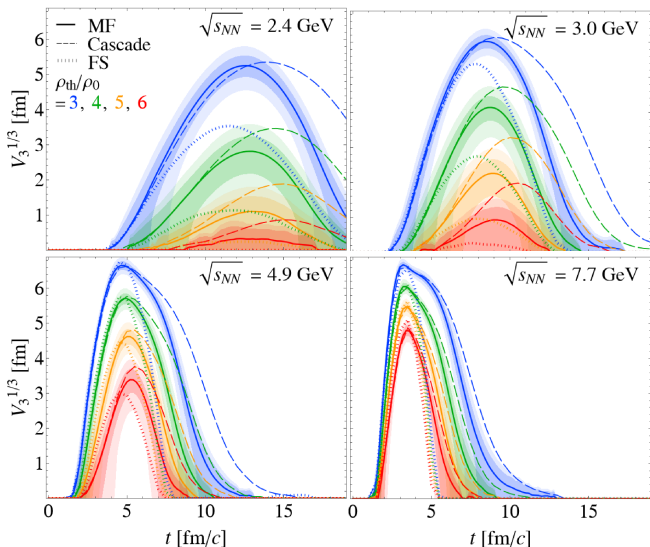


FIG. 1. Time evolution of the spatial volume $V_3(\rho_{\text{th}}; t)$ in central Au+Au collisions for several thresholds ρ_{th} and collision energies $\sqrt{s_{\text{NN}}}$. The thick-solid, dashed, and dotted lines represent MF, Cascade, and FS results, respectively. The color bands around the MF results show the 1σ (denser) and 2σ (lighter) bands of event-by-event fluctuations. At the initial time $t = 0$, the centers of the colliding nuclei are separated by $2R_{\text{Au}}/\gamma_{\text{Au}} + 3$ fm in the longitudinal direction with γ_{Au} being the Lorentz factor for the incident Au ions.

gions with $\rho_{\text{th}}/\rho_0 > 3$ are created with smaller $V_3(\rho_{\text{th}}; t)$, which increase with $\sqrt{s_{\text{NN}}}$. It is also found that the dense region disappears more quickly for larger $\sqrt{s_{\text{NN}}}$.

When comparing MF with Cascade, one finds that $V_3(\rho_{\text{th}}; t)$ is more suppressed in MF. This is because the repulsive mean field [51] makes the matter less compressed [57]. The mean-field effect becomes more important for lower collision energies, especially for $\sqrt{s_{\text{NN}}} \lesssim 3.0$ GeV. The comparison between MF and FS shows that $V_3(\rho_{\text{th}}; t)$ is enhanced by the interaction. Due to the collisions, the particles are decelerated and gather around the collision point, forming a dense region.

In order to examine the $\sqrt{s_{\text{NN}}}$ dependence observed in Fig. 1 quantitatively, we show $\max[V_3(\rho_{\text{th}}; t)]$ and $\tau(\rho_{\text{th}})$ as functions of $\sqrt{s_{\text{NN}}}$ in Fig. 2. It shows that $\max[V_3(\rho_{\text{th}}; t)]$ grows and saturates with increasing $\sqrt{s_{\text{NN}}}$. Meanwhile, $\tau(\rho_{\text{th}})$ decreases except for $\rho_{\text{th}}/\rho_0 \geq 5$ at low collision energies, where the formation of the region with $\rho(x) > \rho_{\text{th}}$ scarcely occurs.

To obtain an observable signal of dense matter, both the spatial volume and the lifetime must be large. The optimal $\sqrt{s_{\text{NN}}}$ to maximize $\max[V_3(\rho_{\text{th}}; t)]$ and $\tau(\rho_{\text{th}})$ simultaneously may be estimated from the crossing point of the solid- and dashed-blue lines in Fig. 2. Taking $\rho_{\text{th}}/\rho_0 = 3$ as an example, it is located at $\sqrt{s_{\text{NN}}} \approx 2.6$ GeV, where a macroscopically large spacetime volume, $\max[V_3(\rho_{\text{th}}; t)]^{1/3} = \tau(\rho_{\text{th}}) \approx 5.5$ fm, is realized. For $\rho_{\text{th}}/\rho_0 = 4$, the crossing point is located at

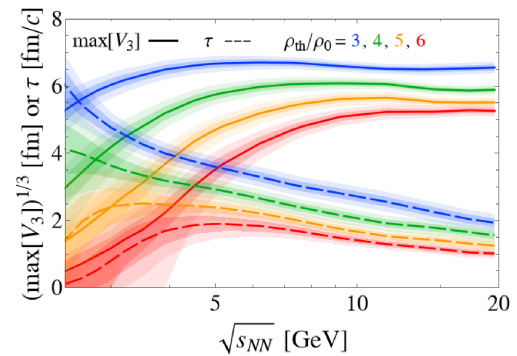


FIG. 2. MF results for the collision energy $\sqrt{s_{\text{NN}}}$ dependence of the maximum volume $\max[V_3]$ (solid) and the lifetime τ (dashed) in central Au+Au collisions. The bands show the event-by-event fluctuations as in Fig. 1.

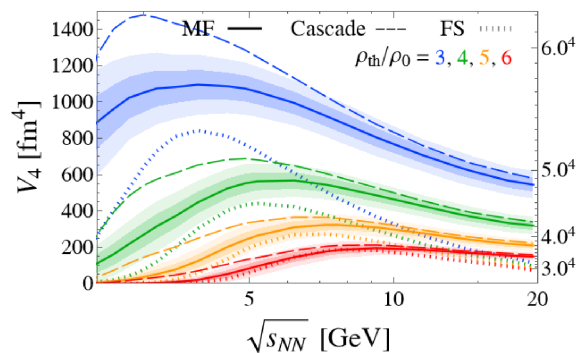


FIG. 3. The collision energy $\sqrt{s_{\text{NN}}}$ dependence of the space-time volume $V_4(\rho_{\text{th}})$ in central Au+Au collisions. The meanings of the lines and bands are the same as Fig. 1.

$\sqrt{s_{\text{NN}}} \approx 2.8$ GeV with $\max[V_3(\rho_{\text{th}}; t)]^{1/3} = \tau \approx 4$ fm, which is smaller than the result for $\rho_{\text{th}}/\rho_0 = 3$, but still occupies a certain spacetime volume of the reaction zone. Similar arguments suggest that an experimental analysis of the matter with $\rho(x)/\rho_0 \gtrsim 5$ is challenging, as $\max[V_3(\rho_{\text{th}}; t)]$ and $\tau(\rho_{\text{th}})$ are suppressed and are no longer macroscopically large.

One can make a similar estimate of the optimal $\sqrt{s_{\text{NN}}}$ from an analysis of the $\sqrt{s_{\text{NN}}}$ dependence of $V_4(\rho_{\text{th}})$, shown in Fig. 3. We estimate the optimal $\sqrt{s_{\text{NN}}}$ with the maximum of $V_4(\rho_{\text{th}})$, which is located around $\sqrt{s_{\text{NN}}} = 4$ and 5.5 GeV for $\rho_{\text{th}}/\rho_0 = 3$ and 4, respectively. These values are slightly higher than those estimated from the crossing points in Fig. 2. The corresponding maximum values are $(V_4(\rho_{\text{th}}))^{1/4} = 5.8$ fm and 4.9 fm, respectively, which are almost the same as the values of $(V_3(\rho_{\text{th}}; t))^{1/3}$ and $\tau(\rho_{\text{th}})$ at the crossing points in Fig. 2.

Wrapping up these results, we conclude that the region with $\rho(x)/\rho_0 \geq 3$ can be formed with macroscopically large spatial and temporal sizes in central Au+Au collisions. The sweet spot of $\sqrt{s_{\text{NN}}}$ to maximize the

spatial and temporal sizes simultaneously starts from $\sqrt{s_{NN}} \lesssim 3$ GeV and extends up to $\sqrt{s_{NN}} \gtrsim 4$ GeV. The optimal collision energy for $\rho(x)/\rho_0 \geq 4$ is estimated to be slightly higher than that for $\rho(x)/\rho_0 \geq 3$. Compared to the previous research, the estimated optimal $\sqrt{s_{NN}}$ is considerably smaller [22, 37]. RemoveAlso, Although the maximum baryon density can locally exceed $\rho(x)/\rho_0 = 8$, as shown in Refs. [35–38], the volume and lifetime of such high baryon-density regions are small.

Finally, we discuss the event-by-event fluctuations. In Figs. 1–3, the colored bands show the 1σ (dense) and 2σ (light) ranges of the event-by-event distribution of the individual quantities. The figures show that $V_3(\rho_{th}; t)$, τ , and $V_4(\rho_{th})$ can fluctuate significantly, which are driven by the positional fluctuation of nucleons on the colliding nuclei [57]. For example, the upper and lower bounds of the 2σ band of $V_4(\rho_{th})$ at $\sqrt{s_{NN}} \lesssim 3$ GeV and $\rho_{th}/\rho_0 = 3$ are 1250 and 850 fm⁴, respectively. In other words, the values of $V_4(3\rho_0)$ in the top and bottom 2.5% collision events differ by a factor of more than $1250/850 \approx 1.5$. This means that, if a selection of such large- and small- V_4 events is available, their comparison is used to investigate the properties of dense matter from the spacetime-volume dependence of experimental observables. As another example, for $\rho_{th}/\rho_0 = 5$, the lower 2σ -bound of $\max[V_3(5\rho_0, t)]$ vanishes at $\sqrt{s_{NN}} \approx 3$ GeV, whereas the upper bound is about $(3 \text{ fm})^3$. Exploiting these large event-by-event fluctuations may allow us to explore even denser regions in the experiments.

Discussions.— We have shown that a high-density matter with $\rho(x)/\rho_0 \gtrsim 3$ can be created with macroscopically large volume at intermediate collision energies. Since $\rho(x)/\rho_0 \gtrsim 3$ is the density expected to be realized in the core of neutron stars [3, 58], it is an important next step to pursue the connection between the two realms. In heavy-ion collisions, observables, such as the directed flow [59, 60], dilepton yields [61–64], and fluctuations of conserved charges [65–67], are expected to be sensitive to the equations of state and the phase transitions. Examining these observables based on our results on the spacetime density profile enables us to further constrain the properties of the matter at baryon densities relevant to neutron stars. In the present study, we have focused on the measures (2)–(4), which do not care about the equilibration of matter. Although this ignorance is the key to realizing the quantitative analysis of the spacetime profile, the consideration of equilibration, as well as the estimation of the resulting temperature and chemical potential, is another important extension of this study to approach the matter properties in equilibrium [57].

Let us discuss the validity of our JAM simulation, which (1) is based on the particular choice of the mean field, i.e., RQMDv with a soft momentum-dependent potential, and (2) is a hadronic model, containing no explicit quark and gluon degrees of freedom. Regarding the choice of the mean field (1), we have also ex-

cuted JAM with other mean field parameters, such as a hard momentum-dependent potential and momentum-independent potentials [51], for comparison. We have found that the choice of the mean field for $\sqrt{s_{NN}} > 2.4$ GeV only gives minor differences, which are smaller than that between the MF and Cascade results shown in Figs. 1 and 3 [57]. Thus, we expect that the estimated optimal $\sqrt{s_{NN}}$ is robust against the choice of the mean field. Nevertheless, the above expectation is drawn from the analysis within JAM, and hence it is an interesting subject to study the spacetime volume and the optimal $\sqrt{s_{NN}}$ with other transport models to reinforce our findings. Regarding (2), we note that recent experimental data on elliptic flow suggest that quark-number scaling [68], which is a possible signal of the formation of the quark-gluon plasma, is violated for $\sqrt{s_{NN}} \lesssim 4$ GeV [69–71]. Therefore, at least around the optimal $\sqrt{s_{NN}} \approx 3$ –4 GeV, the quark-gluon plasma is unformed, and hence the hadronic treatment would suffice. One could, nonetheless, argue that the violation of the quark-number scaling does not fully exclude the possibility that the quark-gluon plasma is locally created in the matter. We expect that the inclusion of quark and gluon degrees of freedom will not significantly alter our conclusions, as the fraction of quark deconfinement phase at $\sqrt{s_{NN}} \lesssim 10$ GeV is not so large [26, 72]. Additionally, the phase transition can influence the spacetime evolution of the matter by softening the equations of state, whose impact on the density is found to be small [46]. Nevertheless, it is worthwhile to test those expectations using models that include explicit quark degrees of freedom such as AMPT [73, 74], PHSD [72, 75, 76], PHQMD [26], PACIAE [77], and hybrid models [33, 34, 78–80], and that incorporate the phase transition dynamics such as UrQMD [62, 81–83] and JAM with an advanced option [46].

We comment on the relation of this study with the event-by-event analysis of fluctuations in conserved charges [65–67]. The large fluctuations of the spacetime volume shown in Figs. 1–3 may fake signals of the fluctuation observables, which are important for the search for the QCD critical point. Taming the fluctuations of the spacetime volume, which would in part be regarded as the volume fluctuations [84, 85], may be crucial in this energy range.

Summary.— We have investigated the volume and lifetime of the high baryon-density matter created in central Au+Au collisions by introducing the three measures (2)–(4) and estimated the optimal collision energy to realize the largest spacetime volume using a microscopic transport model JAM. The numerical results suggest that the dense region with $\rho(x)/\rho_0 \gtrsim 3$ can be created with large volume and lifetime with the optimal collision energy around $\sqrt{s_{NN}} \approx 3$ –4 GeV. These findings are crucial for further investigations of the dense matter with near-future facilities such as NICA, FAIR, HIAF, and J-PARC-HI, as well as the current RHIC BES program.

Acknowledgments.— The authors thank Akira Ohnishi and Toru Nishimura for the collaboration at the early stage of the present work. They also thank Takao Sakaguchi and Hiroyuki Sako for useful discussions. This work is supported by JSPS KAKENHI under grant Nos. 22K14045 and 24K17058 (HT), Nos. JP19H05598, JP22K03619, JP23H04507, and JP24K07049 (MK), No. JP21K03577 (YN), the RIKEN special postdoctoral researcher program (HT), JST SPRING, Grant Number JPMJSP2110 (AJ), the Center for Gravitational Physics and Quantum Information (CGPQI) at Yukawa Institute for Theoretical Physics (MK). A part of the numerical simulations have been carried out on Yukawa-21 at Yukawa Institute for Theoretical Physics (YITP), Kyoto University.

* h.taya@keio.jp

† jinnno@ruby.scphys.kyoto-u.ac.jp

‡ kitazawa@yukawa.kyoto-u.ac.jp

§ nara@aiu.ac.jp

- [1] B. P. Abbott et al. (LIGO Scientific, Virgo), *Phys. Rev. Lett.* **119**, 161101 (2017), 1710.05832.
B. P. Abbott et al. (LIGO Scientific, Virgo, Fermi GBM, INTEGRAL, IceCube, AstroSat Cadmium Zinc Telluride Imager Team, IPN, Insight-Hxmt, ANTARES, Swift, AGILE Team, 1M2H Team, Dark Energy Camera GW-EM, DES, DLT40, GRAWITA, Fermi-LAT, ATCA, ASKAP, Las Cumbres Observatory Group, OzGrav, DWF (Deeper Wider Faster Program), AST3, CAASTRO, VINROUGE, MASTER, J-GEM, GROWTH, JAGWAR, CaltechNRAO, TTU-NRAO, NuSTAR, Pan-STARRS, MAXI Team, TZAC Consortium, KU, Nordic Optical Telescope, ePESSTO, GROND, Texas Tech University, SALT Group, TOROS, BOOTES, MWA, CALET, IKI-GW Follow-up, H.E.S.S., LOFAR, LWA, HAWC, Pierre Auger, ALMA, Euro VLBI Team, Pi of Sky, Chandra Team at McGill University, DFN, ATLAS Telescopes, High Time Resolution Universe Survey, RIMAS, RATIR, SKA South Africa/MeerKAT), *Astrophys. J. Lett.* **848**, L12 (2017), 1710.05833.
B. P. Abbott et al. (LIGO Scientific, Virgo), *Phys. Rev. Lett.* **121**, 161101 (2018), 1805.11581.
B. P. Abbott et al. (LIGO Scientific, Virgo), *Phys. Rev. X* **9**, 011001 (2019), 1805.11579.
- [2] M. C. Miller et al., *Astrophys. J. Lett.* **887**, L24 (2019), 1912.05705.
M. C. Miller et al., *Astrophys. J. Lett.* **918**, L28 (2021), 2105.06979.
T. E. Riley et al., *Astrophys. J. Lett.* **887**, L21 (2019), 1912.05702.
T. E. Riley et al., *Astrophys. J. Lett.* **918**, L27 (2021), 2105.06980.
- [3] R. Kumar et al. (MUSES), *Living Rev. Rel.* **27**, 3 (2024), 2303.17021.
- [4] K. Fukushima and T. Hatsuda, *Rept. Prog. Phys.* **74**, 014001 (2011), 1005.4814.
- [5] K. Nagata, *Prog. Part. Nucl. Phys.* **127**, 103991 (2022), 2108.12423.
- [6] I. Tews, J. Carlson, S. Gandolfi, and S. Reddy, *Astrophys. J.* **860**, 149 (2018), 1801.01923.
- [7] C. Drischler, J. W. Holt, and C. Wellenhofer, *Ann. Rev. Nucl. Part. Sci.* **71**, 403 (2021), 2101.01709.
- [8] H. Koehn et al. (2024), 2402.04172.
- [9] X. Luo, Q. Wang, N. Xu, and P. Zhuang, *Properties of QCD Matter at High Baryon Density* (Springer Nature Singapore, 2022), ISBN 9789811944406.
- [10] <https://home.cern/science/accelerators/large-hadron-collider>.
- [11] J. Chen et al. (2024), 2407.02935.
- [12] J. Adamczewski-Musch et al. (HADES), *Nature Phys.* **15**, 1040 (2019).
- [13] K. Yagi, T. Hatsuda, and Y. Miake, *Quark-gluon plasma: From big bang to little bang*, vol. 23 (2005).
- [14] A. Aparin (STAR Collaboration), *Phys. Atom. Nucl.* **86**, 758 (2023).
- [15] <https://shine.web.cern.ch/>.
- [16] T. Galatyuk, *Nucl. Phys. A* **982**, 163 (2019).
- [17] <https://nica.jinr.ru/>.
- [18] <https://fair-center.de/>.
- [19] <https://english.imp.cas.cn/research/facilities/HIAF/>.
- [20] <https://asrc.jaea.go.jp/soshiki/gr/hadron/jparc-hi/index.html>.
- [21] I. G. Bearden et al. (BRAHMS), *Phys. Rev. Lett.* **93**, 102301 (2004), nucl-ex/0312023.
- [22] J. Randrup and J. Cleymans, *Phys. Rev. C* **74**, 047901 (2006), hep-ph/0607065.
- [23] S. A. Bass et al., *Prog. Part. Nucl. Phys.* **41**, 255 (1998), nucl-th/9803035.
- [24] O. Buss, T. Gaitanos, K. Gallmeister, H. van Hees, M. Kaskulov, O. Lalakulich, A. B. Larionov, T. Leitner, J. Weil, and U. Mosel, *Phys. Rept.* **512**, 1 (2012), 1106.1344.
- [25] J. Weil et al. (SMASH), *Phys. Rev. C* **94**, 054905 (2016), 1606.06642.
- [26] J. Aichelin, E. Bratkovskaya, A. Le Fèvre, V. Kireyeu, V. Kolesnikov, Y. Leifels, V. Voronyuk, and G. Coci, *Phys. Rev. C* **101**, 044905 (2020), 1907.03860.
- [27] Y. B. Ivanov, V. N. Russkikh, and V. D. Toneev, *Phys. Rev. C* **73**, 044904 (2006), nucl-th/0503088.
- [28] Y. B. Ivanov, *Phys. Rev. C* **87**, 064904 (2013), 1302.5766.
- [29] Y. B. Ivanov, *Phys. Rev. C* **87**, 064905 (2013), 1304.1638.
- [30] Y. B. Ivanov, *Phys. Rev. C* **89**, 024903 (2014), 1311.0109.
- [31] H. Petersen, J. Steinheimer, G. Burau, M. Bleicher, and H. Stöcker, *Phys. Rev. C* **78**, 044901 (2008), 0806.1695.
- [32] P. Batyuk, D. Blaschke, M. Bleicher, Y. B. Ivanov, I. Karpenko, S. Merts, M. Nahrgang, H. Petersen, and O. Rogachevsky, *Phys. Rev. C* **94**, 044917 (2016), 1608.00965.
- [33] Y. Akamatsu, M. Asakawa, T. Hirano, M. Kitazawa, K. Morita, K. Murase, Y. Nara, C. Nonaka, and A. Ohnishi, *Phys. Rev. C* **98**, 024909 (2018), 1805.09024.
- [34] J. Cimerman, I. Karpenko, B. Tomasik, and P. Huovinen, *Phys. Rev. C* **107**, 044902 (2023), 2301.11894.
- [35] P. Danielewicz, R. A. Lacey, P. B. Gossiaux, C. Pinkenburg, P. Chung, J. M. Alexander, and R. L. McGrath, *Phys. Rev. Lett.* **81**, 2438 (1998), nucl-th/9803047.
- [36] I. C. Arsene, L. V. Bravina, W. Cassing, Y. B. Ivanov, A. Larionov, J. Randrup, V. N. Russkikh, V. D. Toneev, G. Zeeb, and D. Zschesche, *Phys. Rev. C* **75**, 034902 (2007), nucl-th/0609042.
- [37] A. Ohnishi, *J. Phys. Conf. Ser.* **668**, 012004 (2016),

- 1512.08468.
- [38] P. P. Bhaduri (CBM), PoS **CPOD2021**, 031 (2022).
 - [39] Note1, equation (1) is ill-defined for $J^2 < 0$, which can happen when anti-baryon production occurs. However, anti-baryon production is well suppressed for $\sqrt{s_{NN}} < 20$ GeV. Hence, it is rare to have $J^2 < 0$, and even if it happens the value is very close to zero within the numerical accuracy. Therefore, in our simulation, we simply set $\rho(x) = 0$ if $J^2(x) < 0$.
 - [40] Note2, the integral in Eq. (3) diverges for $\rho_{th} \lesssim \rho_0$, since nuclear matter has the density ρ_0 for $t < 0$ and also nuclear clusters can be formed during heavy-ion reactions, which can survive for a long time. We, thus, limit ourselves to $\rho_{th} > 2\rho_0$, where these effects are negligible.
 - [41] H. Sorge, Phys. Lett. B **373**, 16 (1996), nucl-th/9510056.
 - [42] L. V. Bravina et al., Phys. Lett. B **434**, 379 (1998), nucl-th/9804008.
 - [43] L. V. Bravina et al., Phys. Rev. C **60**, 024904 (1999), hep-ph/9906548.
 - [44] L. V. Bravina, E. E. Zabrodin, S. A. Bass, M. Bleicher, M. Brandstetter, S. Soff, H. Stoecker, and W. Greiner, Phys. Rev. C **62**, 064906 (2000), nucl-th/0011011.
 - [45] L. V. Bravina et al., Phys. Rev. C **78**, 014907 (2008), 0804.1484.
 - [46] Y. Nara, H. Niemi, A. Ohnishi, J. Steinheimer, X. Luo, and H. Stöcker, Eur. Phys. J. A **54**, 18 (2018), 1708.05617.
 - [47] D. E. Kharzeev, J. Liao, S. A. Voloshin, and G. Wang, Prog. Part. Nucl. Phys. **88**, 1 (2016), 1511.04050.
 - [48] Y. Nara, N. Otuka, A. Ohnishi, K. Niita, and S. Chiba, Phys. Rev. C **61**, 024901 (2000), nucl-th/9904059.
 - [49] <https://gitlab.com/transportmodel/jam2>.
 - [50] Y. Nara, A. Jinno, T. Maruyama, K. Murase, and A. Ohnishi, Phys. Rev. C **108**, 024910 (2023), 2306.12131.
 - [51] Y. Nara and A. Ohnishi, Phys. Rev. C **105**, 014911 (2022), 2109.07594.
 - [52] Y. Nara, A. Jinno, K. Murase, and A. Ohnishi, Phys. Rev. C **106**, 044902 (2022), 2208.01297.
 - [53] Note3, in general, the velocity V^μ can receive correction from the mean field [86, 87]. However, we neglect it since we have checked that its effect is well suppressed.
 - [54] C. Fuchs and H. H. Wolter, Nucl. Phys. A **589**, 732 (1995).
 - [55] D. Oliinychenko and H. Petersen, Phys. Rev. C **93**, 034905 (2016), 1508.04378.
 - [56] H. Gao and M. Vanderhaeghen, Rev. Mod. Phys. **94**, 015002 (2022), 2105.00571.
 - [57] H. Taya, A. Jinno, M. Kitazawa, and Y. Nara, in preparation.
 - [58] G. Baym, T. Hatsuda, T. Kojo, P. D. Powell, Y. Song, and T. Takatsuka, Rept. Prog. Phys. **81**, 056902 (2018), 1707.04966.
 - [59] P. K. Sahu, W. Cassing, U. Mosel, and A. Ohnishi, Nucl. Phys. A **672**, 376 (2000), nucl-th/9907002.
 - [60] Y. Nara, H. Niemi, J. Steinheimer, and H. Stöcker, Phys. Lett. B **769**, 543 (2017), 1611.08023.
 - [61] T. Nishimura, M. Kitazawa, and T. Kunihiro, PTEP **2022**, 093D02 (2022), 2201.01963.
 - [62] O. Savchuk, A. Motornenko, J. Steinheimer, V. Vovchenko, M. Bleicher, M. Gorenstein, and T. Galatyuk, J. Phys. G **50**, 125104 (2023), 2209.05267.
 - [63] T. Nishimura, M. Kitazawa, and T. Kunihiro, PTEP **2023**, 053D01 (2023), 2302.03191.
 - [64] T. Nishimura, Y. Nara, and J. Steinheimer, Eur. Phys. J. A **60**, 82 (2024), 2311.14135.
 - [65] M. Asakawa and M. Kitazawa, Prog. Part. Nucl. Phys. **90**, 299 (2016), 1512.05038.
 - [66] X. Luo and N. Xu, Nucl. Sci. Tech. **28**, 112 (2017), 1701.02105.
 - [67] M. Bluhm et al., Nucl. Phys. A **1003**, 122016 (2020), 2001.08831.
 - [68] R. J. Fries, B. Muller, C. Nonaka, and S. A. Bass, Phys. Rev. C **68**, 044902 (2003), nucl-th/0306027.
 - [69] L. Adamczyk et al. (STAR), Phys. Rev. C **88**, 014902 (2013), 1301.2348.
 - [70] L. Adamczyk et al. (STAR), Phys. Rev. C **93**, 014907 (2016), 1509.08397.
 - [71] J. Adam et al. (STAR), Phys. Rev. C **103**, 034908 (2021), 2007.14005.
 - [72] V. P. Konchakovski, E. L. Bratkovskaya, W. Cassing, V. D. Toneev, S. A. Voloshin, and V. Voronyuk, Phys. Rev. C **85**, 044922 (2012), 1201.3320.
 - [73] Z.-W. Lin, C. M. Ko, B.-A. Li, B. Zhang, and S. Pal, Phys. Rev. C **72**, 064901 (2005), nucl-th/0411110.
 - [74] H.-S. Wang, G.-L. Ma, Z.-W. Lin, and W.-j. Fu, Phys. Rev. C **105**, 034912 (2022), 2102.06937.
 - [75] W. Cassing and E. L. Bratkovskaya, Phys. Rev. C **78**, 034919 (2008), 0808.0022.
 - [76] W. Cassing and E. L. Bratkovskaya, Nucl. Phys. A **831**, 215 (2009), 0907.5331.
 - [77] A.-K. Lei, Y.-L. Yan, D.-M. Zhou, Z.-L. She, L. Zheng, G.-C. Yong, X.-M. Li, G. Chen, X. Cai, and B.-H. Sa, Phys. Rev. C **108**, 064909 (2023), 2309.05110.
 - [78] J. Steinheimer and M. Bleicher, Phys. Rev. C **84**, 024905 (2011), 1104.3981.
 - [79] A. Schäfer, I. Karpenko, X.-Y. Wu, J. Hammelmann, and H. Elfner (SMASH), Eur. Phys. J. A **58**, 230 (2022), 2112.08724.
 - [80] M. Ege, J. Mohs, J. Staudenmaier, and H. Elfner (2024), 2409.04209.
 - [81] O. Savchuk, R. V. Poberezhnyuk, A. Motornenko, J. Steinheimer, M. I. Gorenstein, and V. Vovchenko, Phys. Rev. C **107**, 024913 (2023), 2211.13200.
 - [82] P. Li, J. Steinheimer, T. Reichert, A. Kittiratpattana, M. Bleicher, and Q. Li, Sci. China Phys. Mech. Astron. **66**, 232011 (2023), 2209.01413.
 - [83] J. Steinheimer, A. Motornenko, A. Sorensen, Y. Nara, V. Koch, and M. Bleicher, Eur. Phys. J. C **82**, 911 (2022), 2208.12091.
 - [84] V. Skokov, B. Friman, and K. Redlich, Phys. Rev. C **88**, 034911 (2013), 1205.4756.
 - [85] P. Braun-Munzinger, A. Rustamov, and J. Stachel, Nucl. Phys. A **960**, 114 (2017), 1612.00702.
 - [86] G. F. Bertsch and S. Das Gupta, Phys. Rept. **160**, 189 (1988).
 - [87] K. Weber, B. Blaettel, W. Cassing, H. C. Doenges, V. Koch, A. Lang, and U. Mosel, Nucl. Phys. A **539**, 713 (1992).